

# Meta-Modeling for Bias Estimation of Biological Reference Points Under the Schaefer Model

Nicholas Grunloh

February 17, 2022

## Abstract

Stock assessments often assume a two-parameter functional form (e.g., Beverton-Holt or Ricker) for the expected recruitment produced by a given level of spawning output. [Mangel et al. \(2013\)](#) and others have shown that biological reference points such as  $\frac{F^*}{M}$  and  $\frac{B^*}{B(0)}$  are largely determined by a single parameter (steepness) when using two-parameter relationships. These functions introduce strong correlations between reference points (RP) that are pre-determined by the functional form, rather than a biological characteristic of the stock. Mangel et al. note that use of a three-parameter stock-recruitment relationship allows for independent estimation of these reference points. This research seeks to understand the nature of biases in reference points resulting from fitting a two-parameter logistic functional form when the true relationship follows a three-parameter stock-recruitment relationship (SRR). This work demonstrates the useful limits of the misspecified Schaefer model, and the mechanisms of model failure which arise from mapping a three-dimensional parameter space into two dimensions.

# 1 Introduction

The most fundamental model in modern fisheries management is the surplus-production model. These models focus on modeling population growth via nonlinear parametric ordinary differential equations (ODE). Key management quantities called reference points (RP) are derived from the ODE equilibrium equations and depend upon the parameterization of biomass production. Two-parameter parameterizations of the production function have been shown to limit the theoretical domain of RPs (Mangel et al., 2013). The limited RP-space of two parameter models are a major source of model misspecification for RPs and thus induce bias in RP estimation. The behavior of RP estimation bias is not well understood and as a result often underappreciated. A meta-modeling approach is developed here to describe RP biases and explore mechanisms of model failure.

Data for a typical surplus-production model comes in the form of an index of abundance through time which is assumed to be proportional to the reproducing biomass for the population of interest. The index is often observed alongside a variety of other known quantities, but at a minimum, each observed index will be observed in the presence of some known catch for the period.

The observed indices are assumed to have multiplicative log-normal errors, and thus the following observation model arises naturally,

$$I_t = qB_t e^\epsilon \quad \epsilon \sim N(0, \sigma^2). \quad (1)$$

Above  $q$  is often referred to as the “catchability parameter”; it serves as the proportionality constant mapping between the observed index of abundance and biomass.  $\sigma^2$  models residual variation. Biologically speaking  $q$  and  $\sigma^2$  are often treated as nuisance parameters with the “biological parameters” entering the model through a process model on biomass.

Biomass is assumed to evolve as an ODE; in this case I focus on the following form,

$$\frac{dB}{dt} = P(B(t); \boldsymbol{\theta}) - C(t). \quad (2)$$

Here biomass is assumed to change in time by two processes, net production of biomass

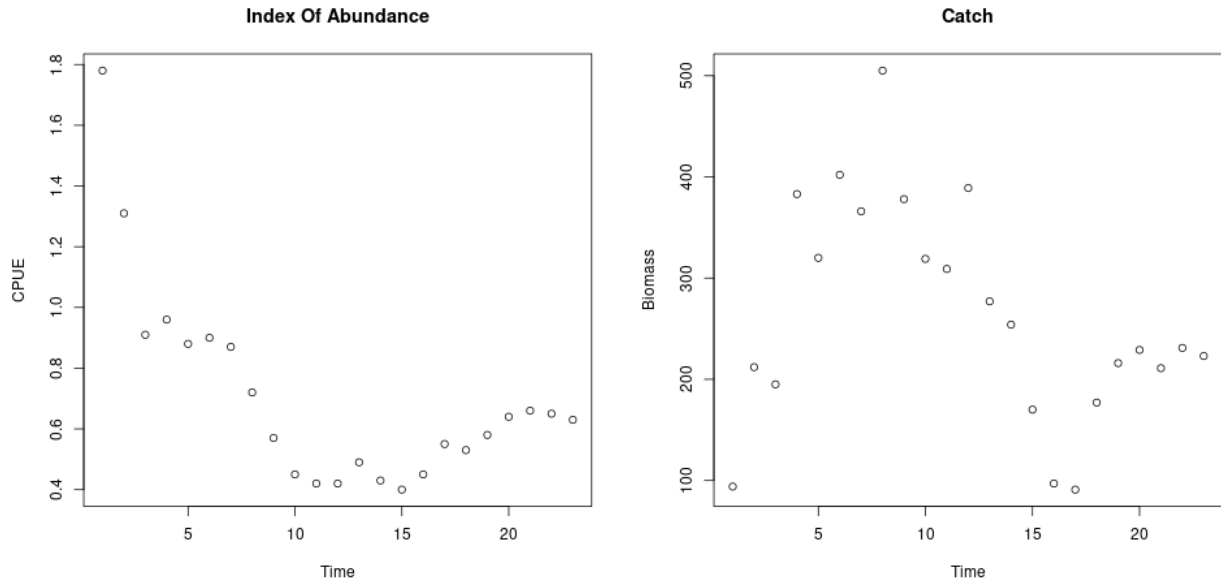


Figure 1: *left*: An observed series of index of abundance data for Namibian Hake from 1965 to 1987 (Hilborn & Mangel, 1997). *right*: The associated catch data for Namibian Hake over the same time period.

into the population, and catches removing biomass from the population.

Firstly, the population grows through a production function,  $P(B)$ . Production in this setting is defined as the net biomass increase due to all reproduction and maturation processes accounting for all naturally occurring sources of mortality other than the recorded fishing from humans. The production function is assumed to be a parametric function that relates the current biomass of the population to an aggregate production of biomass.

Secondly, the population decreases as biomass is removed due to catch,  $C(t)$ . While catches (aka yields) are observable quantities (Pearson & Erwin, 1997), the model assumes that catch is proportional to biomass with the proportionality constant representing the fishing rate,  $F(t)$ , so that  $C(t) = F(t)B(t)$ . From a management perspective a major goal of the model is to accurately infer a quantity known as *maximum sustainable yield* (MSY). One could maximize simple yield at a particular moment in time (and only for that moment) by fishing all available biomass in that moment. This strategy is penny-wise but pound-foolish (not to mention ecologically devastating) since it doesn't leave biomass in the population to reproduce for future time periods. We seek to fish in a way that allows (or even encourages) future productivity in the population. This is

accomplished by maximizing the equilibrium level of catch over time. Equilibrium yield is considered by replacing the steady state biomass ( $\bar{B}$ ) in the assumed form for catch, so that  $\bar{C} = F\bar{B}(F)$ , where  $\bar{\phantom{x}}$  indicates a value at steady state. Naturally the steady state biomass is a function of  $F$ ; we will see a specific example of this in Section (2.2). MSY is found by optimizing  $\bar{C}(F)$  with respect to  $F$ , and  $F^*$  is the fishing rate at MSY. Going forward let  $*$  decorate any value derived under the condition of MSY.

The canonical production model in fisheries is the Schaefer model. The Schaefer model is formed by choosing  $P$  to be logistic growth (Mangel, 2006) parameterized by  $\theta = [r, K]$  so that the family of production functions takes the following form,

$$P(B; [r, K]) = rB \left(1 - \frac{B}{K}\right). \quad (3)$$

$r$  is a parameter controlling the maximum reproductive rate of the population in the absence of competition for resources (i.e. the slope of production function at the origin).  $K$  is the so called "carrying capacity" of the population. In this context the carrying capacity can be formally stated as steady state biomass in the absence of fishing (i.e.  $\bar{B}(0) = K$ ).

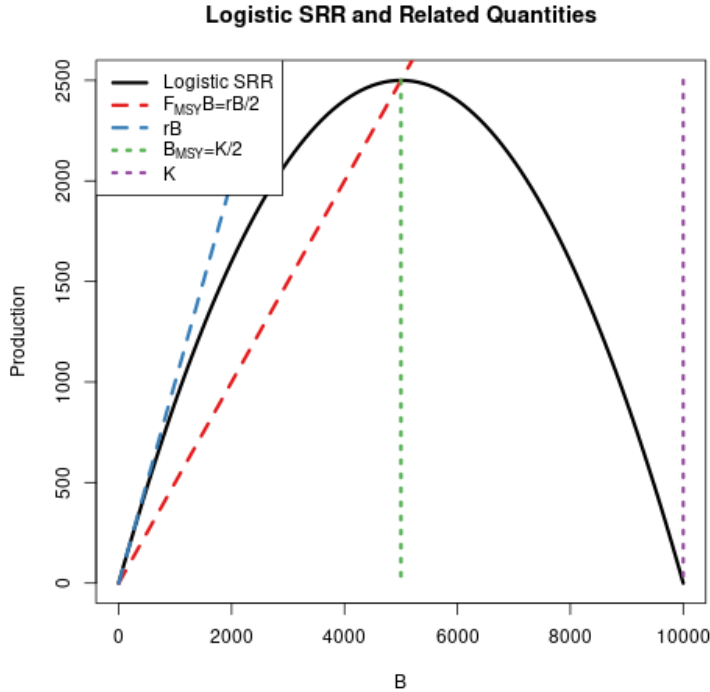


Figure 2:  
The logistic production function in black plotted next to depictions of the key biological parameters and reference points. The slope at the origin (and thus  $r$ ) is shown in blue, catch resulting in MSY in red, biomass at MSY in green, and  $K$  in purple at the right x-intercept. MSY is seen at the peak of the parabola, and is attained with a fishing rate of  $\frac{r}{2}$  and biomass equilibrating to  $\frac{K}{2}$ .

The logistic production function produces idealized parabolic recruitment with equilibrium quantities taking very simple forms that can be easily understood from the graphical construction seen in Figure (2). Positive recruitment is observed when  $B \in (0, K)$ . Due to the parabolic shape of the logistic production function it is straightforward to see that yield is maximized by fishing the stock down to  $B^*$ , where the stock attains its peak productivity. By symmetry it is clear that this peak occurs at  $B^* = \frac{K}{2}$ . The fishing rate required to hold the stock at MSY is  $F^* = \frac{r}{2}$ , which is half of the stock's maximum reproductive rate at the origin. MSY is then the product of  $F^*$  and  $B^*$  so that  $MSY = \frac{rK}{4}$ .

Fisheries are very often managed based upon reference points which serve as simplified heuristic measures of population behavior. The mathematical form of RPs depends upon the model assumptions through the production function. Here the focus is primarily on the RPs  $F^*$  and  $\frac{B^*}{B(0)}$ .

$F^*$  is the afore mentioned fishing rate which results in MSY.  $\frac{B^*}{B(0)}$  is the depletion of the stock at MSY. That is to say  $\frac{B^*}{B(0)}$  describes the fraction of the unfished population biomass that will remain in the equilibrium at MSY. In general  $F^* \in \mathbb{R}^+$  and  $\frac{B^*}{B(0)} \in (0, 1)$ , however under the assumption of logistic production these quantities take the following form,

$$F^* = \frac{r}{2} \qquad \frac{B^*}{B(0)} = \frac{1}{2} \qquad (4)$$

so that  $(F^*, \frac{B^*}{B(0)}) \in (\mathbb{R}^+, \frac{1}{2})$ .

In current practice, production functions are typically chosen to depend only on two parameters. The Schaefer model as presented depends only on the biological parameters  $r$  and  $K$ , but other common two parameter choices of the production function are the Beverton-Holt (Beverton & Holt, 1957, BH) and Ricker (Ricker, 1954) curves. All of these two parameter production functions struggle similarly to model the full theoretical space of RPs (Mangel et al., 2013).

The basis of the Schaefer model is ripe with debate (Kingsland, 1982), and the debate continues within modern fisheries modeling (Prager, 2002). On the one hand, Maunder (2003) argues that the Schaefer model is insufficient in large part due to the

restriction it places on  $\frac{B^*}{B(0)}$ , at  $\frac{1}{2}$ , and further argues that the three parameter Pella-Tomlinson (PT) model (Pella & Tomlinson, 1969) should replace the Schaefer model to avoid biased parameter estimates. On the other hand, while Prager (2003) appreciates the limitations of the Schaefer model, he argues its usefulness as a well understood and simple model that has the ability to reasonably approximate dynamics in many data poor stocks.

The bias-variance trade-off (Ramasubramanian & Singh, 2017) makes it clear that the addition of a third parameter in the production function will necessarily reduce estimation bias. However the utility of this bias reduction is still under debate because the particular mechanisms and behavior (direction and magnitude) of these biases for key management quantities are not fully understood or described. Lee et al. (2012) provides some evidence that estimation of productivity parameters, and thus RPs via (Mangel et al., 2013), are dependent on biomass contrast as well as model specification. Conn et al. (2010) comes to similar conclusions via calibration modeling techniques. Despite this understanding of productivity estimation, the implications have not been extended to a joint description of biases on the scale of management RPs.

Together the general behavior of the PT model and the simplicity of the Schaefer model make the PT/Schaefer pair an ideal setting for beginning to understand the consequences of model misspecification on the production function. In this study I consider the behavior of inference when data are simulated from the three parameter PT production model but fit with the two parameter Schaefer model.

The work begins with a derivation of RPs under the three parameter PT model. The parametric forms of RPs under the PT model are then inverted to develop a simulation setting for analyzing inference under the two parameter Schaefer model. Finally a Gaussian Process (GP) meta-model is constructed for exploration and analysis of RP biases.

A key insight of this approach is that bias is considered broadly across RP-space to uncover patterns and correlations between RPs. The GP meta-model is explicate about trade-offs between RPs so as to inform the full utility of reducing bias, as well suggest mechanisms for understanding what causes bias. Further, the effect of contrast on estimation is considered together with model misspecification.

## 2 Methods

### 2.1 PT Model

The three parameter PT family has a convenient form that includes, among others (Fox Jr., 1970; Rankin & Lemos, 2015), the logistic production function as a special case to form the Schaefer model. The Pella-Tomlinson production function is parameterized so that  $\theta = [r, K, \gamma]$  and the family takes the following form,

$$P(B; [r, K, \gamma]) = \frac{rB}{\gamma - 1} \left(1 - \frac{B}{K}\right)^{\gamma-1}. \quad (5)$$

$\gamma$  is a parameter which breaks PT out of the restrictive symmetry of the logistic curve. In the special case of  $\gamma = 2$  Eq(5) collapses back to the logistic curve, however in general  $\gamma \in (1, \infty)$ . The parameters  $r$  and  $K$  maintain the same interpretation as they do in the logistic production function. In Figure (3) PT recruitment is shown for a range of parameter values so as to demonstrate the various recruitment shapes that can be achieved by PT recruitment.

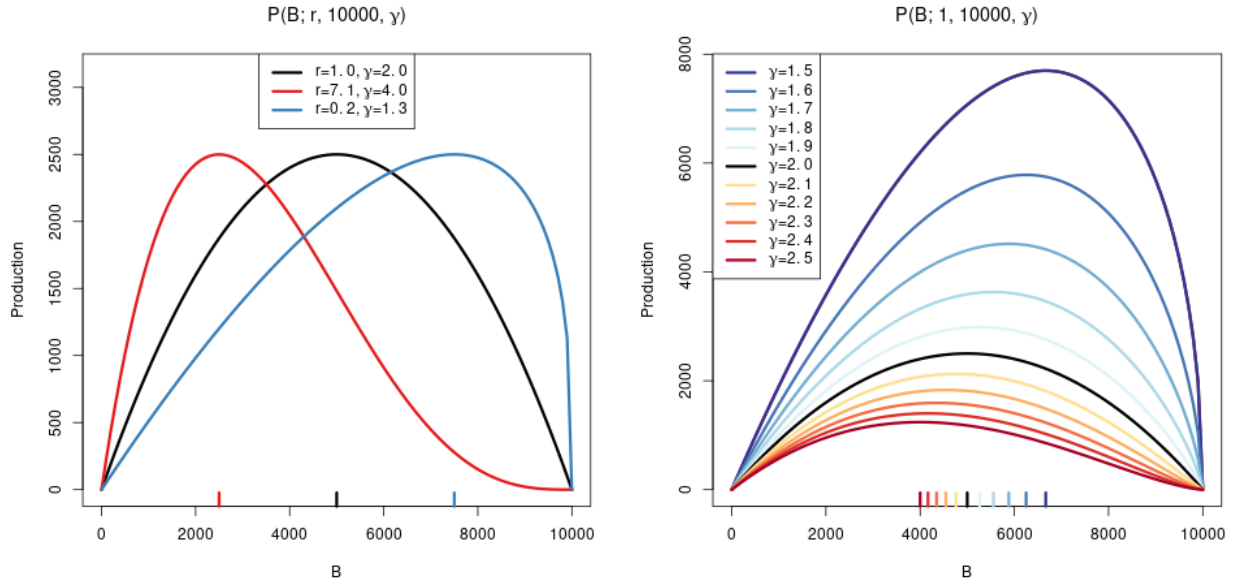


Figure 3: (*left*) PT production functions with parameters chosen so that MSY is consistent, but  $\frac{B^*}{B(0)}$  is less than  $\frac{1}{2}$  (in red), greater than  $\frac{1}{2}$  (in blue), or equal to  $\frac{1}{2}$  (in black; logistic production function). (*right*) PT production functions over a range of  $\gamma$  values with the values of  $r$  and  $K$  fixed at 1 and 10,000 respectively.

While the particular form of how  $\gamma$  appears in PT still produces some limitations to the form of the production function, importantly the introduction of a third parameter allows enough flexibility to fully describe the space of reference points used in management. To see this, the reference points are analytically derived for the PT model below.

## 2.2 PT Reference Points

With  $B(t)$  representing biomass at time  $t$ , under PT production, the dynamics of biomass are defined by the following ODE,

$$\frac{dB}{dt} = \frac{rB}{\gamma - 1} \left(1 - \frac{B}{K}\right)^{\gamma-1} - FB. \quad (6)$$

An expression for the equilibrium biomass is attained by setting Eq(6) equal to zero, and rearranging the resulting equation to solve for  $B$ . Thinking of the result as a function of  $F$  gives,

$$\bar{B}(F) = K \left(1 - \left(\frac{F(\gamma - 1)}{r}\right)^{\frac{1}{\gamma-1}}\right). \quad (7)$$

At this point it is convenient to notice that  $\bar{B}(0) = K$ . The expression for  $B^*$  is given by evaluating Eq(7) at  $F^*$ .

To get an expression for  $F^*$ , the equilibrium yield is maximized with respect to  $F$ ,

$$F^* = \operatorname{argmax}_F F \bar{B}(F). \quad (8)$$

In the case of PT production this maximization can be done analytically (however many three parameter production functions do not result in tractable analytical solutions). In this case maximization can proceed by differentiating the equilibrium yield with respect to  $F$  as follows,

$$\frac{dY}{dF} = \bar{B}(F) + F \frac{d\bar{B}}{dF} \quad (9)$$

$$\frac{d\bar{B}}{dF} = -\frac{K}{F(\gamma - 1)} \left(\frac{F(\gamma - 1)}{r}\right)^{\frac{1}{\gamma-1}}. \quad (10)$$



Setting Eq(9) equal to 0, substituting  $\bar{B}(F)$  and  $\frac{d\bar{B}}{dF}$  by Equations (7) and (10) respectively, and then solving for  $F$  produces the following expression for the fishing rate required to produce MSY,

$$F^* = \frac{r}{\gamma - 1} \left( \frac{\gamma - 1}{\gamma} \right)^{\gamma - 1}. \quad (11)$$

Plugging the above expression for  $F^*$  back into Eq(7) gives the following expression for biomass at MSY,

$$B^* = \frac{K}{\gamma}. \quad (12)$$

The above derived expressions for  $\bar{B}(0)$ ,  $B^*$ , and  $F^*$  can then be used to build a specific analytical form for the biological reference points in terms of only biological model parameters.

$$F^* = \frac{r}{(\gamma - 1)} \left( \frac{\gamma - 1}{\gamma} \right)^{\gamma - 1} \quad \frac{B^*}{\bar{B}(0)} = \frac{1}{\gamma} \quad (13)$$

## 2.3 Simulation Study

Indices of abundance are simulated from the three parameter PT production model over a grid of  $F^*$  and  $\frac{B^*}{\bar{B}(0)}$  values. These PT data are then fit with a two parameter Schaefer model.

Generating simulated indices of abundance from the PT model requires inverting the relationship between  $\left(F^*, \frac{B^*}{\bar{B}(0)}\right)$ , and  $(r, \gamma)$ . It is not generally possible to analytically invert this relationship for many three parameter production functions (Punt & Cope, 2019; J. T. Schnute & Richards, 1998). Most three parameter production functions lead to RPs that require expensive numerical methods to invert; more over the numerical inversion procedure can often be unstable. That said, for the case of PT this relationship is analytically invertible, and leads to the following relationship

$$r = F^* \left( \frac{1 - \frac{B^*}{\bar{B}(0)}}{\frac{B^*}{\bar{B}(0)}} \right) \left( 1 - \frac{B^*}{\bar{B}(0)} \right)^{\left( \frac{\frac{B^*}{\bar{B}(0)} - 1}{\frac{B^*}{\bar{B}(0)}} \right)} \quad \gamma = \frac{1}{\frac{B^*}{\bar{B}(0)}}. \quad (14)$$

Indices are generated under the following conditions. Data are simulated at each point on the grid  $\mathcal{F} \times \mathcal{B}$ , with  $F^* \in \mathcal{F}$  and  $\frac{B^*}{B(0)} \in \mathcal{B}$ , where  $\mathcal{F} = \{0.1, 0.2, \dots, 0.7\}$  and  $\mathcal{B} = \{0.2, 0.3, \dots, 0.6\}$  as seen in Figure (4). These ranges of values for  $F^*$  and  $\frac{B^*}{B(0)}$  are selected to include a wide range of values thought to reflect many commonly assessed fisheries. The red X's in Figure (4) show four simulation locations where the Schaefer model is misspecified to a large degree and will be considered in more detail in Section(3.1). For each  $\left(F^*, \frac{B^*}{B(0)}\right)$ , the associated pair  $(r, \gamma)$  are computed from Eq (14). Since  $K$  does not enter the RP calculation its value is fixed arbitrarily at 10000. The value of  $q$  is fixed at a typically small value of 0.0005.  $\sigma$  is fixed at the relatively small value of 0.01 to focus specifically on the behavior of population parameters. These parameters fully specify the PT model for the purposes of generating index data for each  $\left(F^*, \frac{B^*}{B(0)}\right)$  pair.

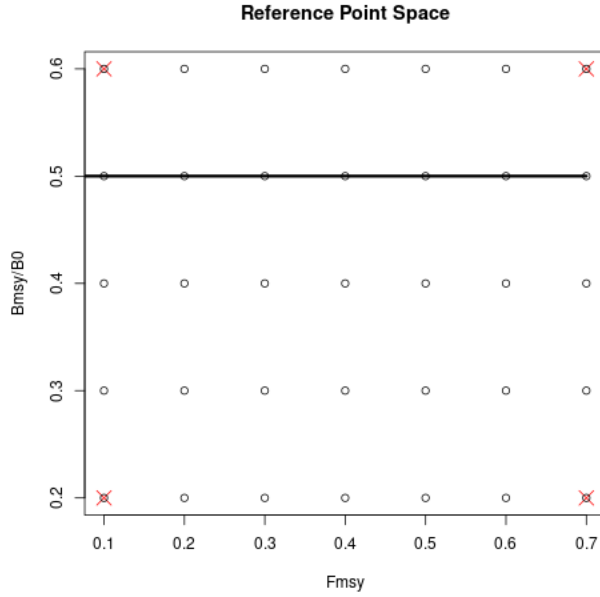


Figure 4: Open circles show the location of the simulation grid  $\mathcal{F} \times \mathcal{B}$ . The horizontal line shows the constrained space of RPs for the Schaefer model. The red X's indicated 4 simulation locations where the Schaefer model is particularly misspecified.

## 2.4 Catch

It is known that the behavior of catch can effect inference on the biological parameters (Hilborn & Walters, 1992). In particular it is thought that catch can induce "contrast" in index data so as to better inform  $r$ . In this setting contrast refers to changes in the long term trends of index data. Figure(8, *right*) demonstrates an example of biomass that includes contrast induced by catch. It is not well understood how contrast may factor into biases induced by model misspecification. To investigate this a variety of catches are investigated.

Catch is parameterized so that  $F(t)$  can be controlled with respect to  $F^*$ . Recall that catch is assumed to be proportional to biomass with the proportionality constant amounting to the fishing rate, so that  $C(t) = F(t)B(t)$ . To control  $F(t)$  with respect to  $F^*$ ,  $C(t)$  is specified by defining the quantity  $\frac{F(t)}{F^*}$  as the relative fishing rate.  $B(t)$  is defined by the solution of the ODE, and  $F^*$  is defined by the biological parameters of the model, see Eq(11). Thus by defining  $\frac{F(t)}{F^*}$ , catch can then be written as  $C(t) = F^* \left( \frac{F(t)}{F^*} \right) B(t)$ .

Intuitively  $\frac{F(t)}{F^*}$  describes the fraction of  $F^*$  that  $F(t)$  is specified to for the current  $B(t)$ . When  $\frac{F(t)}{F^*} = 1$ ,  $F(t)$  will be held at  $F^*$ , and the solution of the ODE brings  $B(t)$  into equilibrium at  $B^*$ . For constant  $\frac{F(t)}{F^*}$  the Schaefer model comes to equilibrium as an exponential decay from  $K$  approaching  $B^*$ . The relative fishing rate is defined on  $[0, \infty)$ ; when  $\frac{F(t)}{F^*} < 1$ ,  $F(t)$  is lower than  $F^*$  and  $B(t)$  is pushed toward  $\bar{B} > B^*$ . Contrarily, when  $\frac{F(t)}{F^*} > 1$ ,  $F(t)$  is higher than  $F^*$  and  $B(t)$  is pushed toward  $\bar{B} < B^*$ ; the precise values of  $\bar{B}$  can be calculated from Eq(7).

In practice, catch is determined by a series of observed, assumed known, catches. Catch observations are typically observed on a quarterly (or yearly) basis, so that the ODE may be discretized via Euler's method with integration step sizes to match the observation frequency of the modeled data. In this case, catch is sampled as would be done in practice however, the simulation can encounter a variate of issues working with the naively discretized ODE. As a result the ODE is integrated implicitly via the Livermore Solver (Radhakrishnan, 1993, lsode), and catch is linearly interpolated between sampled epochs.

## 2.5 Model Fitting

The goal of model fitting is to assess how the biological parameters of the two parameter Schaefer model behave under MLE inference when fit to PT data. Thus, let  $I_t$  be an observation of PT index data at time  $t \in \{1, 2, 3, \dots, T\}$ . The observation model is log-normal such that,

$$I_t|q, \sigma^2, \boldsymbol{\theta} \sim LN(qB_t(\boldsymbol{\theta}), \sigma^2). \quad (15)$$

For the Schaefer model  $\boldsymbol{\theta} = [r, K]$ , and  $B_t(\boldsymbol{\theta})$  is defined by the solution of the following ODE

$$\frac{dB}{dt} = rB \left(1 - \frac{B}{K}\right) - FB. \quad (16)$$

The  $I_t$  are assumed independent conditional on  $q, \sigma^2, r, K$  and the ODE model for biomass. Thus the log likelihood can be written as

$$\log \mathcal{L}(q, \sigma^2, \boldsymbol{\theta}; I) = -\frac{T}{2} \log(\sigma^2) - \frac{1}{2\sigma^2} \sum_t \log \left( \frac{I_t}{qB_t(\boldsymbol{\theta})} \right)^2. \quad (17)$$

In this setting,  $q$  is fixed at the true value of 0.0005 to focus on the inferential effects of model misspecification on biological parameters.  $\sigma^2$ ,  $r$ , and  $K$  are reparameterized into the log scale as  $\log(\sigma^2)$ ,  $\log(r)$ , and  $\log(K)$  and fit via MLE.  $\sigma^2$  is allowed to be fit to assess overall model fit. Reparameterization of the parameters into the log scale improves the reliability of optimization in addition to facilitating the use of Hessian information for parameter estimate standard errors.

Given that the biological parameters enter the likelihood via a nonlinear ODE, and further the parameters themselves are related to each other nonlinearly, the likelihood function can often be difficult to optimize. A hybrid optimization scheme is used to maximize the log likelihood to ensure that a global MLE solution is found. The R package GA ([Scrucca, 2013, 2017](#)) is used to run a genetic algorithm to explore parameter space globally. Optimization occasional jumps into the L-BFGS-B local optimizer to refine optima within a local mode. The scheme functions by searching globally to iteratively improving hot starts for the local optimizer.

In Appendix (7) a profile likelihood method for estimating all of the parameters of the model is derived. The profile likelihood technique greatly improves the reliability of local optimizers when fitting the biological parameters alongside additional nuisance parameters. The catchability parameter  $q$  has the effect of rescaling biomass which can often function similarly to the role of the carrying capacity parameter  $K$ . Thus, the structure of the likelihood may confound  $q$  and  $K$ , and for some data these parameters may only be weakly identifiable. Posing the model in a Bayesian context provides a convenient mechanism for managing these weak identifiability issues. In a tactful Bayesian formulation  $q$  and  $\sigma^2$  may then be marginalized out of the joint posterior to yield fast and reliable inference (Walters & Ludwig, 1994).

## 2.6 Gaussian Process Metamodel

For assessing biological parameters over the simulated grid, as seen in Figure(4), a GP model is used as a flexible, stochastic interpolator over RP space. As previously established, in Section (2.5), the biological parameters of interest are the Schaefer model's  $\log(r)$  and  $\log(K)$  parameters. Since the estimates of these parameters are random variables, with variances given by the inverse of the observed fisher information, interpolation of MLEs requires paying additional attention to propagating estimates of uncertainty into the metamodel.

A GP is a stochastic process generalizing the normal distribution to an infinite dimensional analog. GPs are often specified primarily through the choice of a covariance function which defines the relationship between locations in an index set. Typically the index set is spatial for GPs, and in this setting the model is across the reference point space,  $\left(F^*, \frac{B^*}{B(0)}\right)$ , of the three parameter PT data generating model. A GP model implies an  $n$  dimensional multivariate normal distribution on the observations of the model and the covariance function fills out the covariance matrix for the observations.

Modeling the estimates of  $\log(r)$  and  $\log(K)$  with independent GP models is used to extend analysis of all major biological RP over the simulated grid. Let  $\hat{\mu}$  be the maximum likelihood estimate (MLE) of either  $\log(r)$  or  $\log(K)$ . Additionally let  $\hat{\omega}$  be the inverted Hessian information of the log likelihood evaluated at  $\hat{\mu}$ .

Each grid location of the simulation produces a single fitted  $\hat{\mu}_i$  at an associate  $\left(F^*, \frac{B^*}{B(0)}\right)$  location with  $i \in \{1, \dots, n\}$ .  $\hat{\mu}$  is jointly modeled over the space of reference

points as the following GP,

$$\begin{aligned}
\mathbf{x} &= \left( F^*, \frac{B^*}{\overline{B}(0)} \right) \\
\hat{\mu} &= \beta_0 + \boldsymbol{\beta}' \mathbf{x} + f(\mathbf{x}) + \epsilon \\
f(\mathbf{x}) &\sim \text{GP}(0, \tau^2 R(\mathbf{x}, \mathbf{x}')) \\
\epsilon_i &\sim \text{N}(0, \hat{\omega}_i).
\end{aligned} \tag{18}$$

The GP residual variation provides an ideal mechanism for propagating uncertainty from inference in the simulation step into the metamodel.  $\hat{\omega}_i$  is the observed residual variation for the inferred value,  $\hat{\mu}_i$ . This mechanism down weights the influence of each  $\hat{\mu}_i$  in proportion to the inferred sampling distribution uncertainty. This has the effect of smoothing the GP model in a way similar to the nugget effect ([Gramacy & Lee, 2012](#)).

Here  $R$  is the squared exponential correlation function.

$$R(\mathbf{x}, \mathbf{x}') = \exp \left( \sum_{j=1}^2 \frac{-(x_j - x'_j)^2}{2\ell_j^2} \right) \tag{19}$$

$R$  has an anisotropic separable form to allow for differing length scales in the  $F^*$  and  $\frac{B^*}{\overline{B}(0)}$  axes. The flexibility to model correlations separately in the different RP axes is key due to the differences in the extent of the RP domains marginally.  $\ell_1$  and  $\ell_2$  model the length scales for  $F^*$  and  $\frac{B^*}{\overline{B}(0)}$  respectively. The metamodel parameters  $\beta_0$ ,  $\boldsymbol{\beta}$ ,  $\tau^2$ ,  $\ell_1$  and  $\ell_2$  are fit via MLE against the observations of  $\hat{\mu}$  and  $\hat{\omega}$  from simulation fits.

Predictive estimates of modeled quantities are obtained via kriging over intermediate values over RP space. Let  $\tilde{\cdot}$  decorate any quantity that is derived for metamodel interpolation.

$$\tilde{\mu}(\tilde{s}) = \beta_0 + \mathbf{x}(\tilde{s})\boldsymbol{\beta} + R_{\ell}(\tilde{s}, s)R_{\ell}^{-1}(s, s)\left(\hat{\mu}(s) - (\beta_0 + \mathbf{x}(s)\boldsymbol{\beta})\right) \tag{20}$$

### 3 Results

While interpolation occurs in the space of either  $\log(r)$  or  $\log(K)$ , these interpolated values are used to build interpolated estimates of major biological reference points. Using the interpolated values  $\check{\log}(r)$  and  $\check{\log}(K)$  the following transformation are applied to interpolate RP quantities under the Schaefer model,

$$\check{B}^* = \frac{\check{K}}{2} \quad \check{F}^* = \frac{\check{r}}{2}. \quad (21)$$

Using these interpolated RP quantities, the bias induced by model misspecification is quantified by the following relative measure of bias, similar to a percent error calculation.

$$\text{Relative Bias} = \frac{\check{RP} - RP}{RP} \quad (22)$$

Above  $RP$  is a stand in for the the true value of any of the biological reference points under PT data generation, and  $\check{RP}$  refers to the interpolated estimated RP quantity under the Schaefer model.

#### 3.1 An $MSY$ -Optimal Catch History

When  $F(t)$  is held constant at  $F^*$ ,  $B(t)$  comes to equilibrium as an exponential decay from  $K$  to  $B^*$ . Understanding model misspecification bias is simplified in this setting due to the relative simplicity of  $B(t)$ . However this simplicity is known to poorly inform estimates of  $r$ , and thus  $F^*$ , due to the limited range of the production function that is observed (Hilborn & Walters, 1992). This example is a "low contrast" setting.

Figure(5) shows the biases in  $F^*$  and  $\frac{B^*}{B(0)}$  over the space of simulated RPs. The (*top-right*) panel shows how data generated across a broad space of RPs are mapped onto the limited space of the Schaefer line. Below the Schaefer line, RP estimates are biased by over-estimating  $\frac{B^*}{B(0)}$  and under-estimating  $F^*$ . Above the Schaefer line the vice-versa is true;  $\frac{B^*}{B(0)}$  is under-estimated and  $F^*$  is over-estimated. In the (*left*) and (*bottom*) panels the bias in  $\frac{B^*}{B(0)}$  and  $F^*$  are shown component-wise; each panel showing the same patterns, but focusing on only one component of the bias at a time. In these panels red coloring indicates over-estimation of the RP and blue indicates

under-estimation. Notice that the region of RPs near the Schaefer line enjoy relatively low bias since model misspecification is minor in this region.

Notice that under the Schaefer model, Eq(12) with  $\gamma = 2$ ,  $B^*$  is necessarily half of  $K$ . Since  $\frac{B^*}{B(0)}$  is always  $\frac{1}{2}$  under the Schaefer model, the bias in  $\frac{B^*}{B(0)}$  (as seen in Figure(5)) simply measures the distance from the data generating location vertically to the Schaefer line.

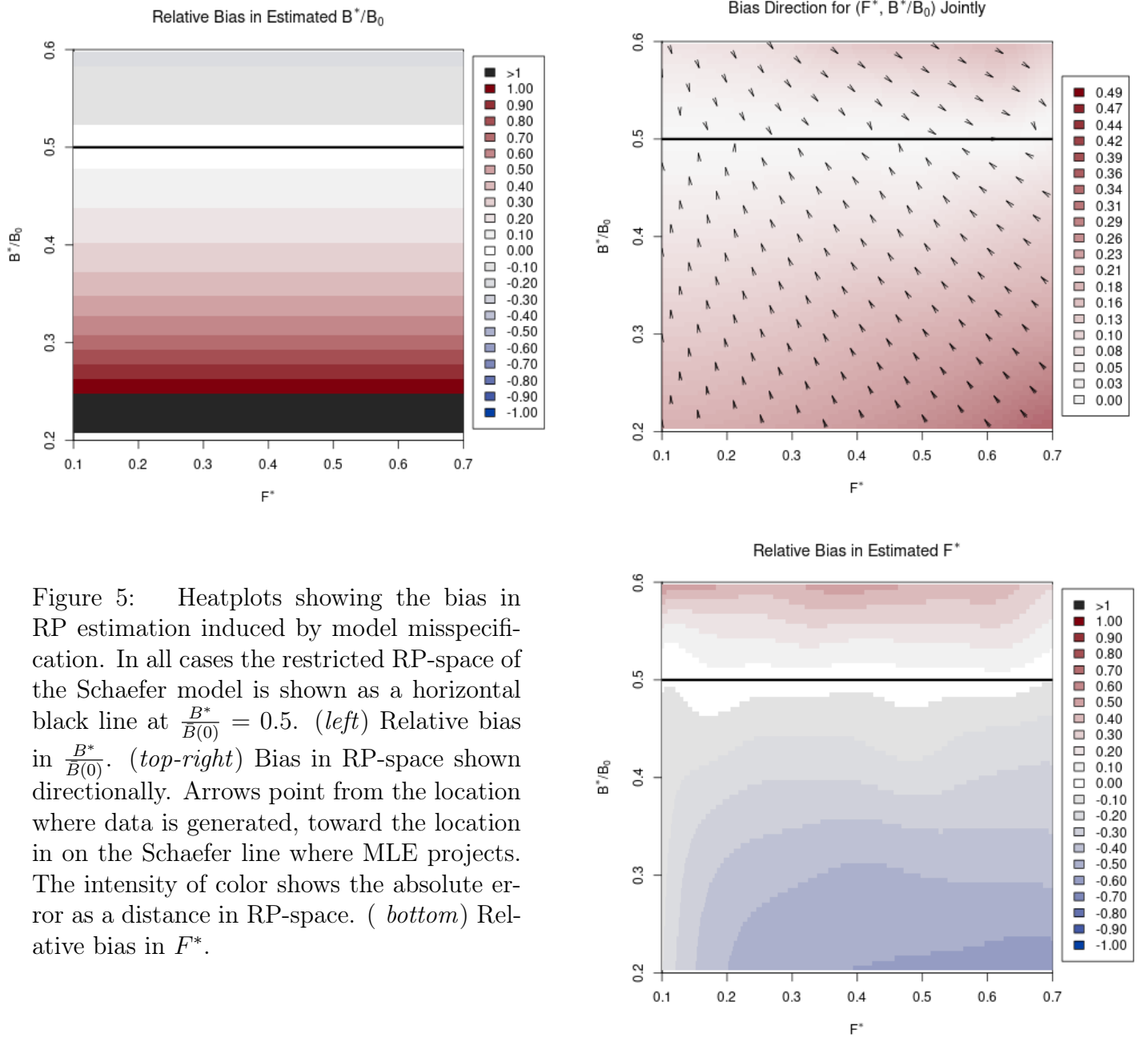


Figure 5: Heatplots showing the bias in RP estimation induced by model misspecification. In all cases the restricted RP-space of the Schaefer model is shown as a horizontal black line at  $\frac{B^*}{B(0)} = 0.5$ . (left) Relative bias in  $\frac{B^*}{B(0)}$ . (top-right) Bias in RP-space shown directionally. Arrows point from the location where data is generated, toward the location in on the Schaefer line where MLE projects. The intensity of color shows the absolute error as a distance in RP-space. (bottom) Relative bias in  $F^*$ .



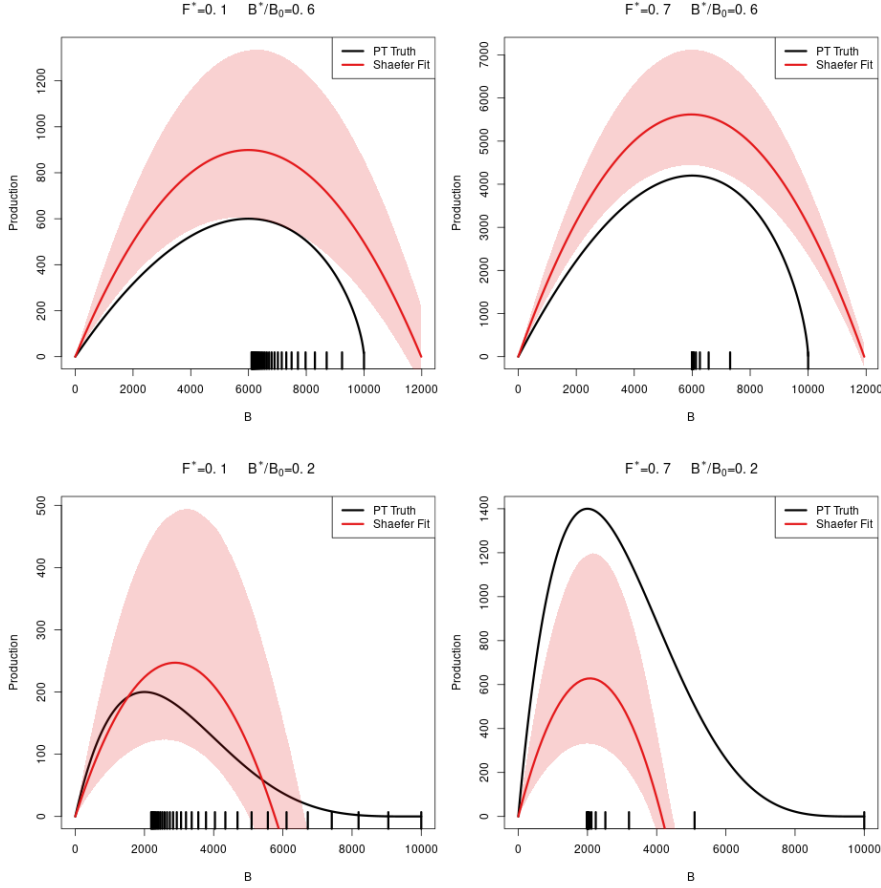


Figure 6: A comparison of the true PT production function (in black) and the estimated logistic curve (in red) with 95% CI shown. The examples shown represent the four corners of maximum model misspecification in the simulated RP-space. Observed biomasses are plotted in the rug plots below the curves.

Figure(6) shows four of the most misspecified example production function fits as compared to the true data generating PT production functions. In the rug plots below each set of curves the observed biomasses demonstrate the exponential decay from  $K$  to  $B^*$  in each case. In particular, notice how only biomasses greater than the PT  $B^*$  are observed. Due to the leaning of the true PT curves, and the symmetry of the logistic parabola, the logistic curve only observes information about its slope at the origin from data observed on the right portion of the PT curves. Above the Schaefer line PT is steeper on the right of  $B^*$  than it is on the left, and so the the logistic curve over-estimates  $r$ , and thus  $F^*$ , for data generated above the Schaefer line. Below the Schaefer line the vice versa phenomena occurs. Below the Schaefer line PT is shallower to the right of  $B^*$  than it is on the left and so the logistic parabola estimate tends to under estimate  $F^*$ .

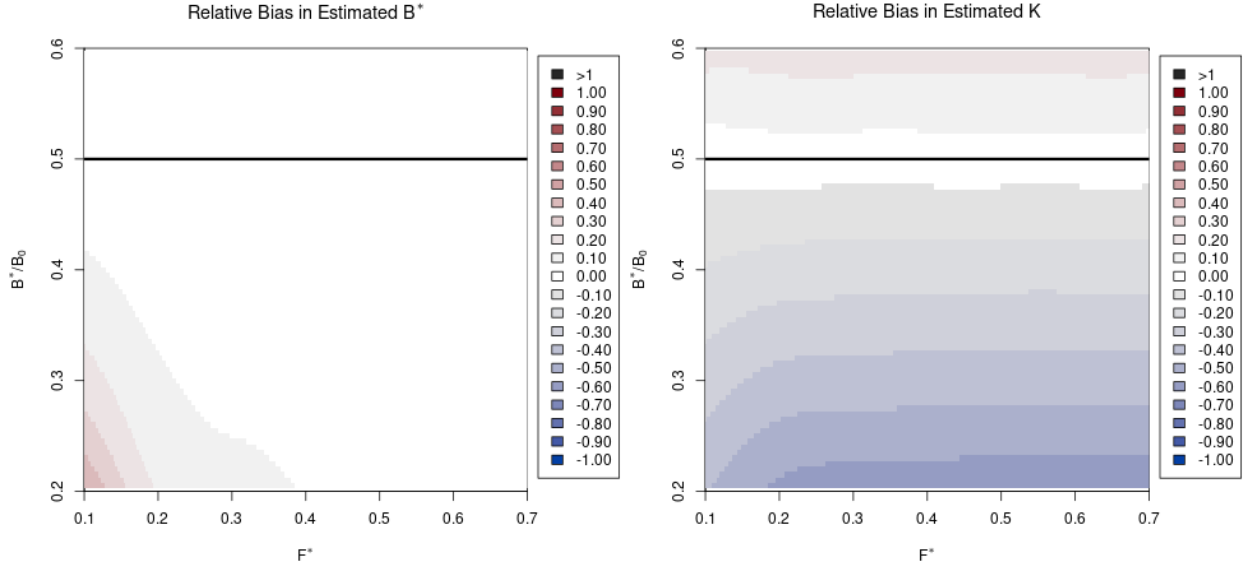


Figure 7: MLE Bias surfaces for  $B^*$  (left) and  $K$  (right) individually.

Figure(6) also gives some examples of the relative behavior of  $B^*$  and  $K$ . In Figure(5) it is clear that the bias behavior of  $\frac{B^*}{B(0)}$  is locked in a fixed pattern under the Schaefer model. Figure(6) indicates that the individual biases of  $B^*$  and  $K$  may behave quite differently.  $B^*$  appears to be estimated fairly accurately while  $K$  does not.

Figure(7) teases apart  $\frac{B^*}{B(0)}$  into individual bias surfaces for  $B^*$  and  $K$  respectively. Interestingly  $B^*$  enjoys a large region of RP-space with relatively low bias. Given that  $B^*$  has relatively consistently low bias,  $K$  maintains the expected inverse relationship with  $\frac{B^*}{B(0)}$  bias. Since the parabolic structure of the logistic function ties the ratio of  $B^*$  and  $\bar{B}(0)$  to  $\frac{1}{2}$ , there is only one degree of freedom shared between  $B^*$  and  $\bar{B}(0)$  so that their ratio is maintained at  $\frac{1}{2}$ . In this setting it appears that  $B^*$  estimation is largely conserved at the cost of  $K$ .

### 3.2 More Informative Catch Histories

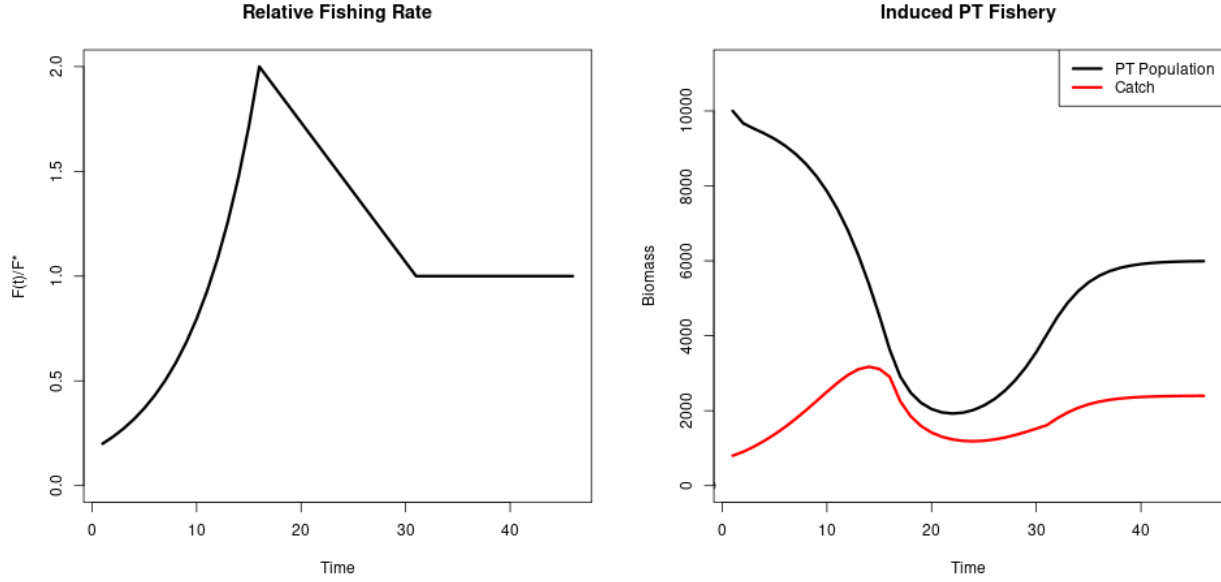


Figure 8: (*left*) Relative fishing specified so as to induce contrast. (*right*) Population biomass and catch demonstrating contrast in a PT population with  $F^* = 0.4$  and  $\frac{B^*}{B(0)} = 0.6$ .

The setting of constant relative fishing rate is a useful simplification for building understanding of the dynamics that induce bias, but in practice constant fishing rate is a somewhat oversimplified setting. Consider a hypothetical stock where fishing rate accelerates as technology and fishing techniques improve rapidly until management practices are applied. Figure(8) demonstrates this more realistic, while still somewhat idyllic, fishing behavior. This population is exposed to a variety of fishing rates, which induce contrast in the generated indices and allow the fitting model to observe the population decrease in size and subsequently rebuild. This represents a "high contrast" setting that is widely thought to better inform growth rate parameters, such as  $r$ .

Figure(9) shows the relative bias surfaces for  $B^*$  and  $F^*$  under 45 epochs of data in the high contrast setting. On the one hand, notice the relative lack of bias in  $F^*$  over a large swath of RPs far from the Schaefer line. On the other hand, notice that bias in  $B^*$  increases here relative to the low contrast setting. The pattern of bias in  $B^*$  maintains a similar pattern, and overall scale, as the low contrast setting seen in Figure(7), however a smaller region of RP-space enjoys low bias here. Due to the

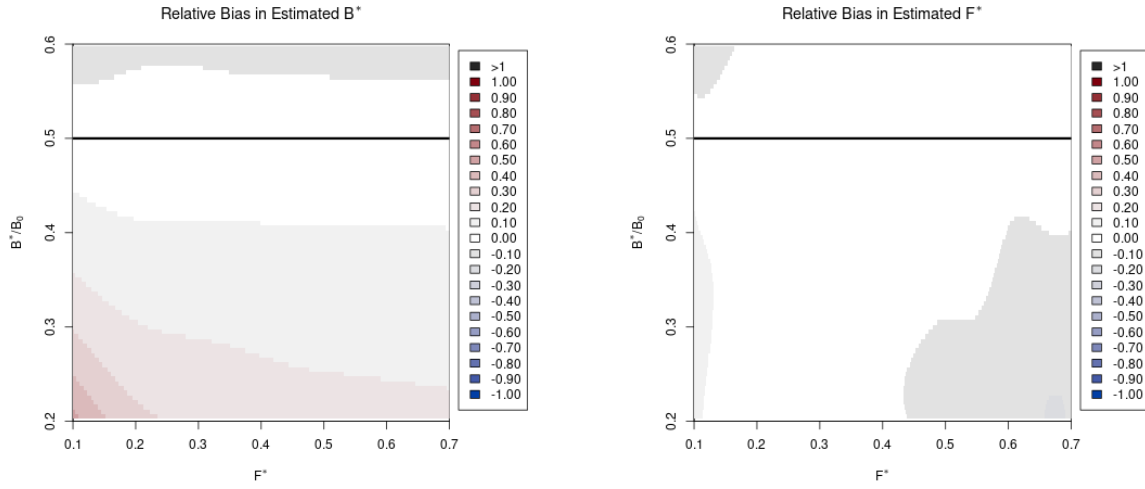


Figure 9: MLE Bias surfaces for  $B^*$  (left) and  $F^*$  (right) with relative fishing rate as specified in Figure(8)

similar, albeit expanded, pattern of  $B^*$  bias here, as compared with the low contrast setting, and the constrained relationship with  $\frac{B^*}{B(0)}$ , the bias surface for  $K$  maintains the same general inverse relationship with  $\frac{B^*}{B(0)}$ .

If the data are augmented so that the fishing rate is held at  $F^*$  for an additional 45 time epochs, so that slower growing stocks may observe more data near  $B^*$ , Figure(10) shows the updated bias surfaces. The scale of bias in  $B^*$  is reduced, but the general patterns of bias remains similar for both RPs. While the bias behavior of  $B^*$  estimates are diminished,  $F^*$  biases are generally magnified.

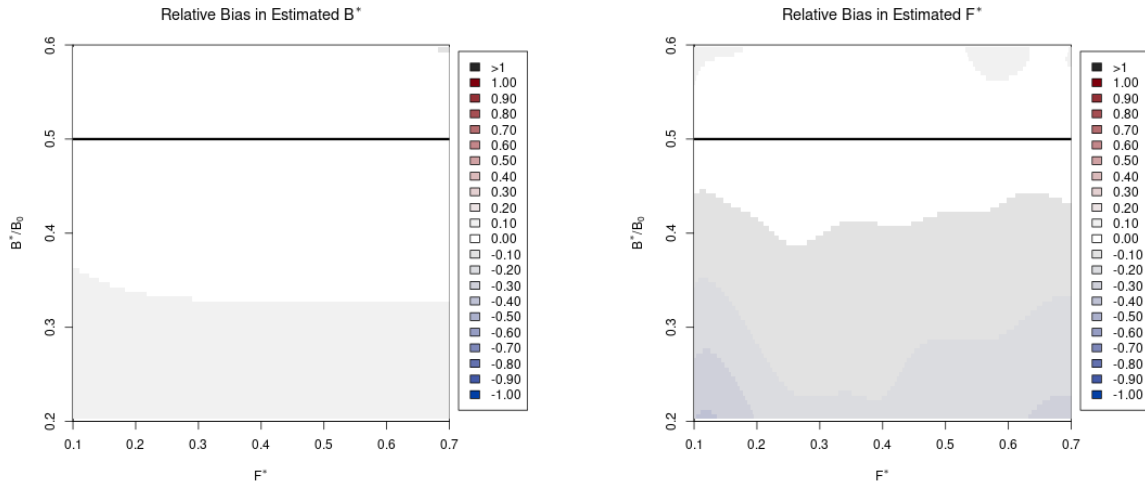


Figure 10: MLE Bias surfaces for  $B^*$  (left) and  $F^*$  (right) with relative fishing rate augmented with additional observations near equilibrium.

## 4 Discussion

Results presented here generally agree with what is known about estimating growth rate parameters (Lee et al., 2012; Conn et al., 2010; Magnusson & Hilborn, 2007), in this case  $r$ , and thus  $F^*$ . In the presence of contrast  $F^*$  estimation can enjoy very low bias even for a wide range of poorly specified models; conversely in the absence of contrast  $F^*$  estimation can suffer very large bias even for slightly misspecified models. In all cases when model misspecification is removed, even with weakly informative data,  $F^*$  estimation is unbiased. Model misspecification is thus a necessary but not sufficient condition for inducing bias.

While it is established that growth rate parameters require contrast to estimate, the implications of these biases jointly across a variety of RPs have not received as much attention. When considering  $B^*$  alongside  $F^*$  in varying contrast environments, it becomes clear that different data informs different parts of the production function differently. In low contrast environments  $B^*$  estimation is remarkably unbiased across all but the most challenging instances of model misspecification. However in the presence of contrast, while  $F^*$  enjoys better estimation,  $B^*$  estimation experiences substantial bias for only modestly misspecified models. Further, by augmenting contrasting data with an additional period of low contrast data this pattern begins to reverse with  $B^*$  bias receding toward more poorly specified models and  $F^*$  bias encroaching toward only modestly misspecified models as seen in Figure (10).

The behavior of bias in estimating  $B^*$  and  $F^*$  suggests that the limited parameter space of the Schaefer model induces a trade off in estimating these parameters. In practice, when the true model is not known and the Schaefer model is unlikely to be correctly specified, one should at best expect to only estimate either  $B^*$  or  $F^*$  correctly depending on the particular degree of model misspecification. The observed contrast then serves to distribute the available information among  $B^*$  and  $F^*$ . Increasing the flexibility of the production function by moving toward curves with additional parameters could release these structural limitations (Mangel et al., 2013). Punt and Cope (2019) considers a suite of possible three parameter curves which could be used instead of current two parameter curves.

This study only explores the compatibility of the possible productivity shapes exhib-

ited by the PT and Schaefer models. While the PT and Schaefer models are instructive for a variety of dome shaped production behaviors, it is possible that under different modeling assumptions, for example BH production or age structured models, different bias patterns will emerge. Extending this work to be able to make claims in those settings is necessary for developing more generally extensible claims.

Given the role that catch plays in understanding where the production function is informed, it is clear that good estimates of catch are important for contextualizing modeling inferences. While the production model treats catches as known without uncertainty, upon inspection of Figure (1, *right*) this assumption is clearly suspect. Results presented here only consider very deterministic catch histories. More work is needed to understand how jittery catch may affect RP estimation. A smoothing model of catch may be preferable for estimation, but results of this study suggest that even improvements to the contextual understanding of catch will be important for interpreting model inferences correctly.

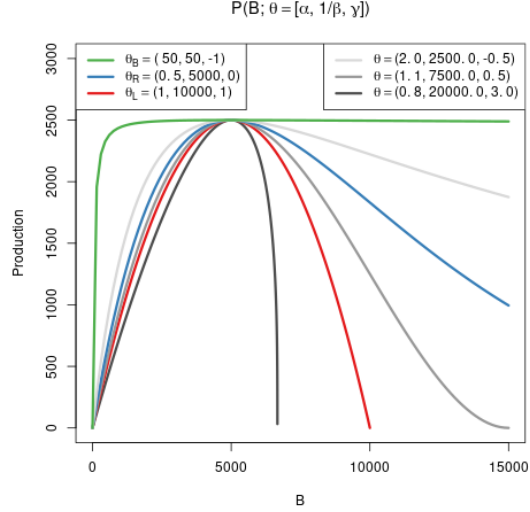
## 5 Productivity and Growth Extensions

The Deriso production function presents a convenient three parameter form that is capable of representing many of the most common two parameter production functions as special cases (Deriso, 1980). The BH and Logistic production functions arise when  $\gamma$  is fixed to -1 or 1 respectively, and the Ricker model is a limiting case as  $\gamma \rightarrow 0$  (J. Schnute, 1985).

$$\frac{dB}{dt} = P(B; \theta) - (M + F)B$$

$$P(B; [\alpha, \beta, \gamma]) = \alpha B(1 - \beta\gamma B)^{\frac{1}{\gamma}}$$

Figure 11: The Deriso production function plotted across a variety of parameter values. The special cases of BH, Ricker, and Logistic production are shown in green, blue, and red respectively.



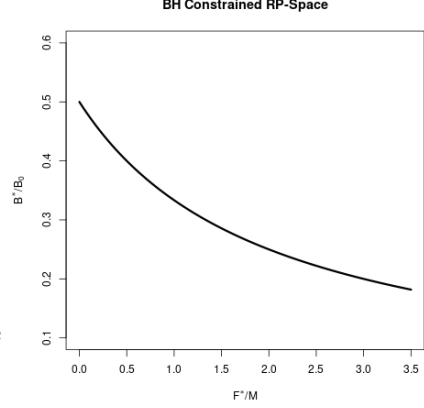
Using the Deriso model as a data generating model across a wide range of RP-space, similarly as described in Section (2.3), presents an ideal setting for extending the above study of RP biases across a broad range of productivity assumptions. Under the Deriso model inverting the relationship between RPs and model parameters is not fully analytically possible (J. T. Schnute & Richards, 1998). Numerical inversion of the nonlinear system seen in Eq (23) is required for determining parameter values for data generation. Notice for a given value of  $\gamma$ ,  $\alpha$  and  $\beta$  can be solved analytically.

$$\begin{aligned} \frac{B^*}{\bar{B}(0)} &= \frac{\left(\frac{\alpha}{M+F^*}\right)^{\frac{1}{\gamma}} - 1}{\left(\frac{\alpha}{M}\right)^{\frac{1}{\gamma}} - 1} \\ \alpha &= (M + F^*) \left[1 - \frac{1}{\gamma} \left(\frac{F^*}{M + F^*}\right)\right]^{-\gamma} \\ \beta &= \frac{1}{\bar{B}(0)} \left(\left(\frac{\alpha}{M}\right)^{\frac{1}{\gamma}} - 1\right) \end{aligned} \tag{23}$$

$$P_{\text{BH}}(B; [\alpha, \beta, -1]) = \frac{\alpha B}{(1 + \beta B)}$$

$$\frac{B^*}{\bar{B}(0)} = \frac{1}{\frac{F^*}{M} + 2}$$

Figure 12: The restricted RP-space under the BH production function.



Inference under the BH model is of particular interest due to its overwhelming popularity. Similar to the limited RP-space of the Schaefer model the two parameter BH model also has a limited RP-space as shown in Figure (12). While the BH constrained RP space is now more complicated than the Schaefer model, analogy to the results obtained under the PT-Schaefer simulation setting, and the flexible GP metamodel, should expedite the analysis of BH inference.

## 5.1 Individual Growth

It is also necessary to study RP bias in the context of individual growth and age-structure. The Deriso-Schnute delay-difference (DD) model provides a compact representation of simple age-structured dynamics (Deriso, 1980; J. Schnute, 1985, 1987). While various modeling strategies may be considered for including effects of age-structure in the population, the Deriso-Schnute DD model presents an ideal model for the simulation setting presented here. The compact representation of the Deriso-Schnute DD model via delay-differential equations accounts for the effects of individual growth and maturity while maintaining relatively fast computation.

The DD model is derived directly from an assumption of Von Bertalanffy growth (Von Bertalanffy, 1938) in weight, Eq(27). In this setting Von Bertalanffy growth relates individual age to individual weight by assuming linear instantaneous growth (as parameterized by the growth parameters  $\kappa$  and  $w_\infty$ ). The DD model expands the idea of biomass production into the processes of recruitment, individual growth, and maturity. This formulation separates the number of individuals in the population ( $N$ ) from the biomass of the population ( $B$ ). The dynamics of  $N$ , as seen in Eq (25), are



very similar to that of the Deriso production model presented above, however the role of the production function is now filled by a "recruitment" function which describes how new individuals are added to the numbers equation. The  $B$  dynamics, can then be seen to describe biomass by an account of 1) biomass of new recruits, 2) the growth of existing biomass, and 3) biomass lost due to mortality. The model accounts for maturity as knife-edge maturity at the instant an individual reaches age  $a_0$ .

$$\frac{dB}{dt} = \overbrace{w(a_0)R(B;\theta)}^{\text{Recruitment Biomass}} + \overbrace{\kappa[w_\infty N - B]}^{\text{Net Growth}} - \overbrace{(M + F)B}^{\text{Mortality}} \quad (24)$$

$$\frac{dN}{dt} = R(B;\theta) - (M + F)N \quad (25)$$

$$R(B; [\alpha, \beta, \gamma]) = \alpha B(t - a_0)(1 - \beta \gamma B(t - a_0))^{\frac{1}{\gamma}} \quad (26)$$

$$w(a) = w_\infty(1 - e^{-\kappa a}) \quad (27)$$

For the purpose of inference the parameters  $\kappa, w_\infty, a_0$  and  $M$  are typically fixed at values determined by the population of study. Thus the primary inferential goal of the DD model is again focused on learning the recruitment parameters. Using the Deriso-Schnute DD model as a data generating model across a wide range of RP-space, and fitting those data under a BH restriction of the DD model, further extends the simulation study of RP bias to include the effects of individual growth.

## 6 Catch Interpolation

The assumption of known catch without uncertainty is suspect, see Figure (1, *right*). While methods for quantifying catch uncertainty have been developed (Shelton et al., 2012), the effect of uncertainty in catch has not been incorporated in stock assessment models (Methot & Wetzel, 2013).

The theoretical use of splines for smoothly and accurately approximating the solution of initial value problems has been well established (Ahlberg et al., 1967). As a statistical model splines are also well established as a nonparametric (or semiparametric) regression technique (Green & Silverman, 1993; Hastie et al., 2009). The use of splines in these two settings, along with the advent of estimates of uncertainty in catch, suggests splines as a useful modeling paradigm for incorporating elements of catch uncertainty into single species stock assessment models.

As previously described in Section (2.4), catch estimates are typically attained on a discrete basis which is matched by the fixed step size discretization of the motivating ODE. Despite a host of numerical issues that naive discretizations can cause, forward Euler discretization of dynamics is largely implemented for convenience for use with discretely sampled data such as catch. For inference (when parameters are not known in advanced) a continuous handling of biomass dynamics largely avoids the numerous numerical issues brought about by naive time stepping. However, a continuous approach requires tactful methodology for moving catch estimates from the current yearly estimates to the interpolated instantaneous quantities needed for a continuous handling of biomass dynamics. Below I propose such a method for interpolating and smoothing catch.

Let  $\tau_j$  represent the starting point of the  $j^{th}$  epoch and let  $t$  represent continuous times falling between the  $\tau$ s. The observed catch at  $\tau_i$  is then  $y(\tau_i)$  and the  $y$  values at epoch boundaries represent the integral of landed biomass from  $\tau_{i-1}$  to  $\tau_i$ . The instantaneous landings,  $x(t)$ , are then modeled as a spline between the epochs as follows,

$$\mathbb{E}[y(t)] = \int_{\tau}^t x(t^*) dt^* \quad \tau = \lceil t \rceil - 1 \quad (28)$$

$$x(t) = \beta_0 + \sum_{j=1}^{T-1} \beta_j (t - \tau_j) \mathbb{1}_{t > \tau_j}. \quad (29)$$

$x(t)$  is a latent model of instantaneous catches. The time integral represents a change of basis of the  $x(t)$  spline model. When the  $y(\tau_i)$  arrive on regular unit epoch intervals, and the time integrals are collapsed, the following observation model for  $y(\tau_i)$  arrives naturally.

$$y(\tau_i) = \beta_0 + \sum_{j=1}^{i-1} \beta_j \left[ \left( \frac{\tau_i^2}{2} - \tau_j \tau_i \right) \mathbb{1}_{\tau_i > \tau_j} - \left( \frac{\tau_{i-1}^2}{2} - \tau_j \tau_{i-1} \right) \mathbb{1}_{\tau_{i-1} > \tau_j} \right] + \epsilon_i \quad (30)$$

$$\beta_j \sim N(0, \phi) \quad \phi \sim \text{Half-Cauchy}(0, 1) \quad \epsilon_i \sim N(0, \sigma_i^2)$$

This representation is nice for several reasons. Firstly, since the accruals of catch are represented as a time integral the resulting model on  $y$  remains linear in  $\beta$ ; in fact this approach results in another spline model on  $y$ , albeit represented in a different basis. Secondly, by explicitly modeling  $x(t)$  with a spline it gives direct interpretability of the  $\beta$ s as slopes of instantaneous catch.

It is worth noting that smoothing in this setting is accomplished by utilizing the observation uncertainty in catch and pooling that information among the  $\beta$ . If all of the  $\sigma_i$  are assumed to be 0 (as would be implied by assuming perfectly known catch) the linear spline becomes fully determined and there is no room for any smoothing. Figure (13) demonstrates model fit with and without uncertainty assumed in catch. Notice that in the absence of catch uncertainty (the blue fit), the  $x(t)$  model must steeply oscillate in order to model jittery observations, while the black model fit, which assumes observation uncertainty, filter out jitters and smoothly explain the data.

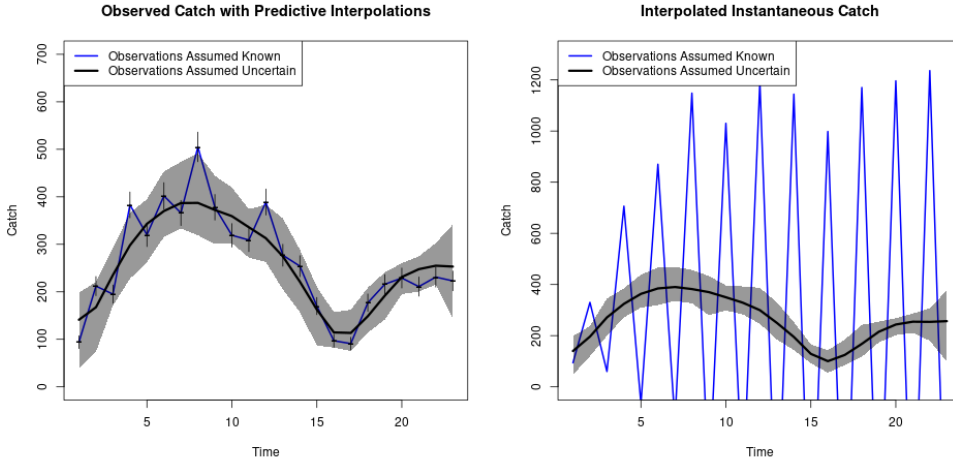
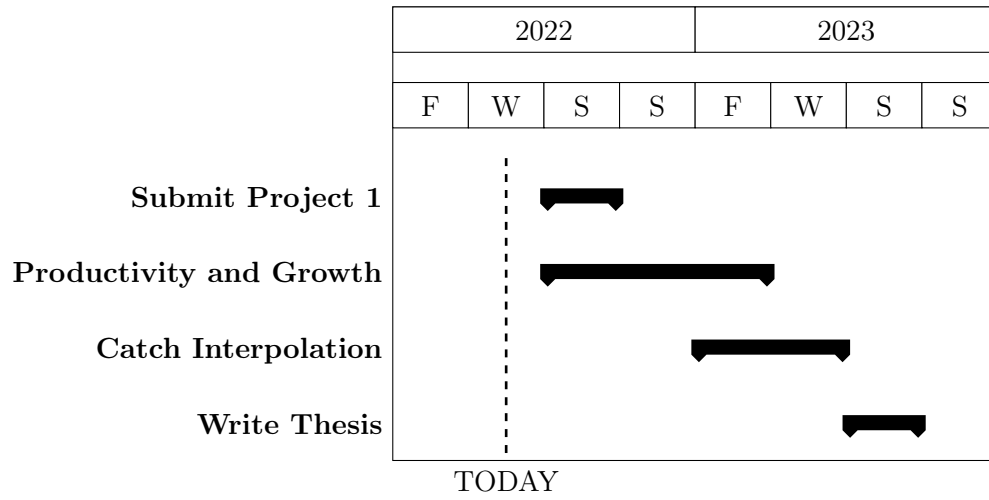


Figure 13:  
(left) Namibian Hake yearly catch observations plotted along with predictive model fits.  
(right) Posterior estimates of instantaneous catch with and without assumed uncertainty in observed catch.

The model fit attained under the assumption of complete certainty in catch clearly leads to defective instantaneous catch behavior. However when uncertainty is added to catch a very sensible catch pattern is reconstructed. Comparison of catch estimates seen directly above in Figure (13) with the catches simulated in Figure (8), from the synthetic high-contrast example, show that this spline method clearly reconstructs a high contrast signal from Namibian hake catches. Given the parsimonious process oriented derivation of this model, these observations suggests that the assumption of certainty among catches is poor.

I propose that this modeling paradigm presents a useful tool for propagating catch uncertainty into the dynamics of stock assessment models. Firstly this method provides a flexible, and interpretable, method for smoothing catch jitters. Secondly this modeling paradigm allows for use with the robust continuous representation of biomass dynamics. A further exploration of smoothing splines, beyond linear basis functions (for example cubic), will be explored. Additionally, the effect of accounting for catch uncertainty with this approach will be evaluated in the context of inference on biomass dynamics parameters.

## 7 Timeline



## References

- Ahlberg, J. H., Nilson, E. N., & Walsh, J. L. (1967). The theory of splines and their applications. *Mathematics in science and engineering*.
- Beverton, R. J., & Holt, S. J. (1957). *On the dynamics of exploited fish populations* (Vol. 11). Springer Science & Business Media.
- Conn, P. B., Williams, E. H., & Shertzer, K. W. (2010). When can we reliably estimate the productivity of fish stocks? *Canadian Journal of Fisheries and Aquatic Sciences*, 67(3), 511–523.
- Deriso, R. B. (1980, February). Harvesting Strategies and Parameter Estimation for an Age-Structured Model. *Canadian Journal of Fisheries and Aquatic Sciences*, 37(2), 268–282. Retrieved 2020-05-13, from <https://www.nrcresearchpress.com/doi/abs/10.1139/f80-034> doi: 10.1139/f80-034
- DeYoreo, M. (2012). *Integrating catchability out of the likelihood*.
- Fox Jr., W. W. (1970). An Exponential Surplus-Yield Model for Optimizing Exploited Fish Populations. *Transactions of the American Fisheries Society*, 99(1), 80–88. Retrieved 2022-02-17, from <https://onlinelibrary.wiley.com/doi/abs/10.1577/1548-8659%281970%2999%3C80%3AAESMFO%3E2.0.CO%3B2> (\_eprint: <https://onlinelibrary.wiley.com/doi/pdf/10.1577/1548-8659%281970%2999%3C80%3AAESMFO%3E2.0.CO%3B2>) doi: 10.1577/1548-8659(1970)99<80:AESMFO>2.0.CO;2
- Gramacy, R. B., & Lee, H. K. (2012). Cases for the nugget in modeling computer experiments. *Statistics and Computing*, 22(3), 713–722. (Publisher: Springer)
- Green, P. J., & Silverman, B. W. (1993). *Nonparametric regression and generalized linear models: a roughness penalty approach*. Crc Press.
- Hastie, T., Tibshirani, R., & Friedman, J. (2009). The Elements of Statistical Learning. *Cited on*, 33.

- Hilborn, R., & Mangel, M. (1997). *The Ecological Detective: Confronting Models with Data*. Princeton University Press.
- Hilborn, R., & Walters, C. J. (1992). Quantitative Fisheries, Stock Assessment: Choice Dynamics, and Uncertainty Chapman and Hall. *New York*.
- Kingsland, S. (1982). The refractory model: the logistic curve and the history of population ecology. *The Quarterly Review of Biology*, 57(1), 29–52. (Publisher: Stony Brook Foundation, Inc.)
- Lee, H.-H., Maunder, M. N., Piner, K. R., & Methot, R. D. (2012, August). Can steepness of the stock–recruitment relationship be estimated in fishery stock assessment models? *Fisheries Research*, 125-126, 254–261. Retrieved 2022-01-29, from <https://linkinghub.elsevier.com/retrieve/pii/S0165783612001099> doi: 10.1016/j.fishres.2012.03.001
- Magnusson, A., & Hilborn, R. (2007). What makes fisheries data informative? *Fish and Fisheries*, 8(4), 337–358. (Publisher: Wiley Online Library)
- Mangel, M. (2006). The Theoretical Biologist’s Toolbox: Quantitative Methods for Ecology and Evolutionary Biology..
- Mangel, M., MacCall, A. D., Brodziak, J., Dick, E., Forrest, R. E., Pourzand, R., & Ralston, S. (2013, April). A perspective on steepness, reference points, and stock assessment. *Canadian Journal of Fisheries and Aquatic Sciences*, 70(6), 930–940. Retrieved 2019-07-03, from <https://www.nrcresearchpress.com/doi/10.1139/cjfas-2012-0372> doi: 10.1139/cjfas-2012-0372
- Maunder, M. N. (2003). Is it time to discard the Schaefer model from the stock assessment scientist’s toolbox? *Fisheries Research*, 61(1-3), 145–149.
- Methot, R. D., & Wetzel, C. R. (2013, May). Stock synthesis: A biological and statistical framework for fish stock assessment and fishery management. *Fisheries Research*, 142, 86–99. Retrieved 2019-11-22, from <https://linkinghub.elsevier.com/retrieve/pii/S0165783612003293> doi: 10.1016/j.fishres.2012.10.012
- Pearson, D. E., & Erwin, B. (1997). Documentation of California’s commercial

- market sampling data entry and expansion programs.
- Pella, J. J., & Tomlinson, P. K. (1969). A generalized stock production model. *Inter-American Tropical Tuna Commission Bulletin*, 13(3), 416–497.
- Prager, M. H. (2002). Comparison of logistic and generalized surplus-production models applied to swordfish, *Xiphias gladius*, in the north Atlantic Ocean. *Fisheries Research*, 58(1), 41–57. (Publisher: Elsevier)
- Prager, M. H. (2003, March). Reply to the Letter to the Editor by Maunder. *Fisheries Research*, 61(1), 151–154. Retrieved 2022-01-30, from <https://www.sciencedirect.com/science/article/pii/S0165783602002746> doi: 10.1016/S0165-7836(02)00274-6
- Punt, A. E., & Cope, J. M. (2019, September). Extending integrated stock assessment models to use non-depensatory three-parameter stock-recruitment relationships. *Fisheries Research*, 217, 46–57. Retrieved 2019-07-19, from <http://www.sciencedirect.com/science/article/pii/S0165783617301819> doi: 10.1016/j.fishres.2017.07.007
- Radhakrishnan, K. (1993). Description and Use of LSODE, the Livermore Solver for Ordinary Differential Equations. , 124.
- Ramasubramanian, K., & Singh, A. (2017). *Machine learning using R* (No. 1). Springer.
- Rankin, P. S., & Lemos, R. T. (2015, October). An alternative surplus production model. *Ecological Modelling*, 313, 109–126. Retrieved 2022-02-11, from <https://www.sciencedirect.com/science/article/pii/S0304380015002732> doi: 10.1016/j.ecolmodel.2015.06.024
- Ricker, W. E. (1954). Stock and recruitment. *Journal of the Fisheries Board of Canada*, 11(5), 559–623. (Publisher: NRC Research Press Ottawa, Canada)
- Schnute, J. (1985, March). A General Theory for Analysis of Catch and Effort Data. *Canadian Journal of Fisheries and Aquatic Sciences*, 42(3), 414–429. Retrieved 2020-05-13, from <https://www.nrcresearchpress.com/doi/abs/10.1139/f85-057> doi: 10.1139/f85-057

- Schnute, J. (1987). A general fishery model for a size-structured fish population. *Canadian Journal of Fisheries and Aquatic Sciences*, 44(5), 924–940. (Publisher: NRC Research Press Ottawa, Canada)
- Schnute, J. T., & Richards, L. J. (1998, February). Analytical models for fishery reference points. *Canadian Journal of Fisheries and Aquatic Sciences*, 55(2), 515–528. Retrieved 2020-01-14, from <https://www.nrcresearchpress.com/doi/abs/10.1139/f97-212> doi: 10.1139/f97-212
- Scrucca, L. (2013, April). GA: A Package for Genetic Algorithms in R. *Journal of Statistical Software*, 53, 1–37. Retrieved 2022-01-17, from <https://doi.org/10.18637/jss.v053.i04> doi: 10.18637/jss.v053.i04
- Scrucca, L. (2017). On Some Extensions to GA Package: Hybrid Optimisation, Parallelisation and Islands Evolution. On some extensions to GA package: hybrid optimisation, parallelisation and islands evolution. *The R Journal*, 9(1), 187–206. Retrieved 2022-01-17, from <https://journal.r-project.org/archive/2017/RJ-2017-008/index.html>
- Shelton, A. O., Dick, E. J., Pearson, D. E., Ralston, S., & Mangel, M. (2012). Estimating species composition and quantifying uncertainty in multispecies fisheries: hierarchical Bayesian models for stratified sampling protocols with missing data. *Canadian journal of fisheries and aquatic sciences*, 69(2), 231–246.
- Von Bertalanffy, L. (1938). A quantitative theory of organic growth (inquiries on growth laws. II). *Human biology*, 10(2), 181–213. (Publisher: JSTOR)
- Walters, C., & Ludwig, D. (1994). Calculation of Bayes posterior probability distributions for key population parameters. *Canadian Journal of Fisheries and Aquatic Sciences*, 51(3), 713–722. (Publisher: NRC Research Press Ottawa, Canada)



## Appendix A: Profile Likelihood MLE

Given that  $q$  has the effect of rescaling the mean function, a naive handling of  $q$  has the potential to interfere with the inference on  $\boldsymbol{\theta}$ . While the parameter  $q$  is typically identifiable, it can introduce lesser modes which complicate naive inference.

Below I outline a profile likelihood method for MLE inference on  $q$  and  $\sigma^2$ . However if posed in a Bayesian context,  $q$  and  $\sigma^2$  may be marginalized out of the joint posterior to yield a direct sampling scheme for  $q$  and  $\sigma^2$  which factors the posterior into the form  $p(q, \sigma^2, \boldsymbol{\theta}|I) = N(\log(q)|\sigma^2, \boldsymbol{\theta}, I)IG(\sigma^2|\boldsymbol{\theta}, I)p(\boldsymbol{\theta}|I)$  (Walters & Ludwig, 1994; DeYoreo, 2012)

The joint likelihood on the log scale can be written as,

$$\log \mathcal{L}(q, \sigma^2, \boldsymbol{\theta}; I) = -\frac{T}{2} \log(\sigma^2) - \frac{1}{2\sigma^2} \sum_t \log \left( \frac{I_t}{qB_t(\boldsymbol{\theta})} \right)^2. \quad (31)$$

First Eq(31) is maximized with respect to  $q$  by partial differentiation of Eq(31) with respect to  $q$ ,

$$\frac{\partial \log \mathcal{L}}{\partial q} = -\frac{1}{q\sigma^2} \left( \sum_t \log \left( \frac{I_t}{B_t(\boldsymbol{\theta})} \right) - T \log(q) \right) \quad (32)$$

The maximum of the likelihood in the  $q$  direction is attained when  $\frac{\partial \log \mathcal{L}}{\partial q} = 0$ . By setting  $\frac{\partial \log \mathcal{L}}{\partial q}$  to 0 and solving for  $q$ , the MLE of  $q$  in terms of  $\boldsymbol{\theta}$  can be written as

$$q(\boldsymbol{\theta}) = e^{\frac{1}{T} \sum_t \log \left( \frac{I_t}{B_t(\boldsymbol{\theta})} \right)} = \left( \prod_t \frac{I_t}{B_t(\boldsymbol{\theta})} \right)^{\frac{1}{T}}. \quad (33)$$

Notice that  $\hat{q}(\boldsymbol{\theta})$  is the geometric mean of the empirical scaling factors between the observed index and modeled biomass at each time. This form is emblematic of the interpretation of the  $q$  parameter as the proportionality constant between the observed index and the modeled biomass. Additionally notice that  $\hat{q}$  is a function of  $\boldsymbol{\theta}$ , so that achieving the global maximum of the likelihood function still requires maximization over  $\boldsymbol{\theta}$ . Furthermore,  $\hat{q}(\boldsymbol{\theta})$  is only a function of  $\boldsymbol{\theta}$  and that  $\sigma^2$  does not enter the expression. This will be helpful in further maximization of the likelihood with respect to  $\sigma^2$ .

Now to maximize in the  $\sigma^2$  direction Eq(31) is differentiated with respect to  $\sigma^2$ ,

$$\frac{\partial \log \mathcal{L}}{\partial \sigma^2} = -\frac{T}{2\sigma^2} + \frac{1}{2(\sigma^2)^2} \sum_t \log \left( \frac{I_t}{qB_t(\boldsymbol{\theta})} \right)^2. \quad (34)$$

The maximum of the likelihood in the  $\sigma^2$  direction is attained when  $\frac{\partial \log \mathcal{L}}{\partial \sigma^2} = 0$ . Setting  $\frac{\partial \log \mathcal{L}}{\partial \sigma^2}$  to 0 and solving for  $\sigma^2$  produces the following MLE as a function of  $\boldsymbol{\theta}$ ,

$$\sigma^2(\boldsymbol{\theta}) = \frac{1}{T} \sum_t \log \left( \frac{I_t}{q(\boldsymbol{\theta})B_t(\boldsymbol{\theta})} \right)^2 \quad (35)$$

Notice that the conditionally MLE of  $\sigma^2$  is not only a function of  $\boldsymbol{\theta}$  but also a function of  $q$ . As previously noted,  $q(\boldsymbol{\theta})$  is only a function of  $\boldsymbol{\theta}$ , and so to achieve a global maximum of the joint likelihood,  $\sigma^2(\boldsymbol{\theta})$  is written entirely in terms of  $\boldsymbol{\theta}$  by replacing  $q$  by  $q(\boldsymbol{\theta})$  as seen above.

By combining Eq(33) and Eq(35) the MLEs of  $q$  and  $\sigma^2$  can be written entirely in terms of  $\boldsymbol{\theta}$ . Furthermore, this realization allows the joint maximization of the likelihood to be reduced to the following profile log-likelihood,

$$\log \mathcal{L}(\boldsymbol{\theta}; I) = -\frac{T}{2} \log(\sigma^2(\boldsymbol{\theta})) - \frac{1}{2\sigma^2(\boldsymbol{\theta})} \sum_t \log \left( \frac{I_t}{q(\boldsymbol{\theta})B_t(\boldsymbol{\theta})} \right)^2. \quad (36)$$

This profile log-likelihood is maximized numerically over  $\boldsymbol{\theta}$ , and the estimates for  $q$  and  $\sigma^2$  are given by evaluating Equations (33) and (35) at  $\hat{\boldsymbol{\theta}}$ .

$$\hat{\boldsymbol{\theta}} = \underset{\boldsymbol{\theta}}{\operatorname{argmax}} \log \mathcal{L}(\boldsymbol{\theta}; I) \quad (37)$$

$$\hat{\sigma}^2 = \sigma^2(\hat{\boldsymbol{\theta}}) \quad (38)$$

$$\hat{q} = q(\hat{\boldsymbol{\theta}}) \quad (39)$$

This profile formulation via  $\hat{q}(\boldsymbol{\theta})$  and  $\hat{\sigma}^2(\boldsymbol{\theta})$  reduces the computational complexity of this numerical optimization, while also avoiding the multimodality issues induced by  $q$ .